Manipulating TDP43 Aggregation via RNA G-quadruplexes

[#]Emily G. Oldani, [#]Kevin M. Reynolds Caicedo, McKenna E. Spaeth Herda, Adam H. Sachs, *Erich G. Chapman, *Sunil Kumar, *Daniel A. Linseman, *Scott Horowitz

[#]Contributed equally, listed alphabetically.

*co-corresponding: erich.chapman@gmail.com, sunil.kumar97@du.edu, daniel.linseman@du.edu, scott.horowitz@du.edu

ABSTRACT

The events that lead to protein misfolding diseases are poorly understood. Many proteins implicated in neurodegenerative diseases (e.g., TDP43) interact with nucleic acids, including RNA G-quadruplexes. In this work, we investigate whether RNA G-quadruplexes play a role in TDP43 aggregation in biophysical and cellular models. We find that G-quadruplexes modulate TDP43 aggregation in a biophysical model and in multiple cell types, including yeast, HEK293T, and motor-neuron-like NSC-34 cells. In yeast cells, treatment with G-quadruplexes causes increased TDP43 accumulation in cells before cellular death. In HEK293T cells expressing TDP43, incubation with G-quadruplex-binding small molecules induces a reduction in chemically-induced TDP43 aggregation. Finally, in NSC-34 cells overexpressing TDP43, we show that G-quadruplexes co-localize with TDP43 aggregates under stress conditions and treatment with G-quadruplex-binding small molecules decreases TDP43-mediated toxicity. Together, these findings suggest that a novel approach to treating protein misfolding diseases may be to target specific RNA structures such as G-quadruplexes.

INTRODUCTION

Trans-active response DNA binding protein 43 kDa (TDP43), is involved in numerous steps of RNA metabolism and regulation for many transcripts[1–5]. It is primarily present and active in the nucleus but can be found in the cytoplasm, even in healthy cells[6–8]. TDP43 inclusions are found in multiple neurodegenerative diseases, including cystic fibrosis, amyotrophic lateral sclerosis (ALS), frontotemporal lobar degeneration (FTLD), and chronic traumatic encephalopathy (CTE)[1,2,9–16]. Aggregation of wild type (WT) TDP43 is a hallmark of sporadic amyotrophic lateral sclerosis, which accounts for nearly 90% of ALS cases, yet the mechanism of this aggregation remains unknown[17].

Based on the RNA-binding capacity of TDP43, using RNA to chaperone TDP43 has been tried in several contexts. For example, TDP43 cytotoxicity was rescued by the expression of human long non-coding RNA (lncRNA) NEAT1 in *Saccharomyces cerevisiae* and in HEK293T cells[17–19]. In yeast, the deletion of debranching enzyme DBR1, and the resulting cytoplasmic build-up of lariat introns, has been observed to reduce the toxicity of TDP43[20]. Additionally, short oligonucleotides with well-characterized TDP43 binding capacity, such as Clip_34nt, have been shown to ameliorate neurotoxic aggregation[21,22].

In addition to its consensus GU-rich binding sequence, TDP43 has been shown previously to bind G-quadruplexes (G4s)[23]. Quadruplexes are four-stranded helices in which guanine forms tetrads, stabilized by cations running through the center of the tetrad stack. Notably, a SELEX experiment found that the binding to G4s was tightest in cases where the TDP43 could not effectively bind its evolved binding partner. While the authors suggested that TDP43 could bind and transports G-quadruplex-containing mRNAs into neurites for local translation, it is also possible that the SELEX experiment was to a misfolded form of TDP43[24–26]. A study testing the effects of short oligonucleotides on TDP43 aggregation and toxicity suggested G4s could mitigate the toxicity of TDP43 in cells[23]. Recently, it was shown that RNA G4s (rG4s) are formed preferentially in cells under cellular stress, as is likely to occur in neurodegenerative disease[27,28]. In addition to binding TDP43, rG4s have recently been shown to have an outsized effect on the aggregation of many proteins[29,30]. Therefore, we sought to explore whether modulating rG4s could affect TDP43 aggregation and toxicity.

RESULTS

In vitro aggregation of TDP43 and G4s

Although it has been previously shown that G4s can bind to TDP43, the ability for G4s to directly modulate TDP43 aggregation was unclear. Therefore, we performed *in vitro* aggregation assays with TDP43 and G4s *(Figure 1a,b).* To test different states of TDP43 as starting points for aggregation, we isolated both the dimer peak and a small aggregate peak from the SEC at the end of protein purification.

LTRIII DNA (5' GGGAGGCGTGGCCTGGGCGGGACTGGGG 3'), a G4 previously demonstrated to have potent chaperone activity[31], was selected to screen with TDP43 and labeled with 6FAM on the 3' end. The G4 LTRIII-FAM was then mixed with 50 μM eGFP-TDP43 aggregate as separated by size exclusion chromatography (*Supplementary Figure 1*), and monitored for aggregation and disaggregation via absorbance at 395 nm *(Figure 1 a,b, Supplementary Figure 2).* As a control, when the G4 was added to the 50 μM eGFP, there was little change in the turbidity *(Supplementary Figure 2).* The untreated eGFP-TDP43 aggregate, however, continued to increase in turbidity over time, eventually visibly precipitating out of solution (*Figure 1a, Supplementary Figure 2*). However, the addition of 10 μM of the G4 LTRIII-6FAM DNA oligomer decreased the turbidity of the eGFP-TDP43 aggregate and prevented the protein from precipitating out of solution (*Figure 1a,b, Supplementary figure 2*). Together, these results show that the G4 was able to prevent the aggregation of the recombinant eGFP-TDP43 *in vitro*, and suggested the ability to disaggregate small TDP43 aggregates.

TDP43 Cytotoxicity rescue in yeast

To test the ability for G4s to affect protein aggregation in cells, we developed a cytotoxicity assay using flow cytometry (*Figure 1c inset*). WT TDP43 is cytotoxic in yeast[8]. There exist known genetic rescues of TDP43 cytotoxicity in yeast; for example, the overexpression of SIS1, and the deletion of debranching enzyme 1 (DBR1)[32,33]. SIS1 is a chaperone protein endogenously expressed in *S. cerevisiae*. DBR1 is a debranching enzyme that debranches lariat RNAs; without it, these lariats are not decayed and consequently build up in the cytoplasm[18,33]. As previously shown, these controls decreased TDP43 cytotoxicity in yeast as measured by spot titers (*Supplementary Figure 3*), in a manner that was not dependent on the use of a DsRED tag (*Supplementary Figure 4*)[34].

Using flow cytometry, we quantified the number of cells that were either dying without high TDP43 expression (*Figure 1c inset,* top left quadrant), dying after tolerating high TDP43 expression (*Figure 1c inset,* top right quadrant) or surviving with high TDP43 expression (*Figure 1c inset,* bottom right quadrant). We then used this technique to quantify the amount of accumulated TDP43-DsRED, comparing WT protein and two disease point mutants, Q331K and D169G[35], and domain deletion ΔNTD of TDP43. However, when measured by cell cytometer, the previously found controls that rescued toxicity by spotting assay did not increase in the amount of WT TDP43 in cells, suggesting that these do not work primarily by stabilizing TDP43. As a result, we looked to other potential strategies to stabilize TDP43 in cells using G4s.

Effects of G4s on TPD43 accumulation in yeast

For comparison with G4s, we tested the effects of two known RNAs that bind TDP43 as part of its regular splicing function, Cy5-AUG12 RNA (5' GUGUAUUGAUUG 3') and Cy5-GU12 RNA (5' GUGUGUGUGUGU 3'), both of which showed an increase in the accumulated TDP43 levels. Before testing the effects of G4s on TDP43 in yeast, the presence of the far-red nuclear death stain DRAQ7, and the 6FAM labeled G4s in the yeast cells were also confirmed by confocal microscopy, as was the expressing of DsRED-tagged protein (*Supplementary Figure 6*). When TDP43-DsRED expressing yeast were co-incubated with G4 DNA displaying previously identified chaperone activity, LTRIII or seq576 seq576 (5' TGTCGGGCGGGGAGGGGGGG 3')[31], the amount of G4 accumulated before cell death increased at similar levels to the evolved TDP43 binders (*Figure 1c*). The amount of TDP43 present in cells also increased as a function of time incubated with the G4 (*Figure 1d)* and as a function of G4 concentration (*Figure 1e*). These results suggest that in yeast, TDP43 can be stabilized by either G4s or evolved binding sequences as part of its splicing function. Next, we wanted to test whether targeting G4s intracellularly using small molecules could aid in TDP43 aggregation and toxicity in a more physiological system, and for these experiments we moved to mammalian cells.

G-quadruplex-binding small molecules (G4 binders) attenuate the aggregation of WT TDP43 in HEK293T cell models

After demonstrating the ability of two G4s to modulate TDP43 aggregation *in vitro* and in yeast model systems, we next examined the effects of G4s on TDP43 aggregation in mammalian cell models. We first developed an oxidative stress model of TDP43 aggregation using stable overexpression of WT TDP43 tagged with YFP[36] in HEK293T cells (HEK293T-TDP43-YFP). We induced oxidative stress in the stably transfected cells using sodium arsenite and observed distinct nuclear aggregation of the TDP43-YFP that overlapped with staining using an antibody to TDP43, consistent with previous TDP43 aggregation studies[37] *(Supplementary Figure 7a*). To confirm this effect was dependent on overexpression of TDP43, HEK293T cells over-expressing an empty vector YFP tag were subjected to the same oxidative stress and no aggregates were observed (*Supplementary Figure 7b).* To observe the timeline of aggregate formation, we performed confocal live-cell imaging over eight h (*Supplementary Figure 7c*). In response to incubation with 50 μM sodium arsenite, TDP43 puncta formed within four h, and continued to form and grow over the course of the experiment. These experiments demonstrated a mammalian model for the nuclear aggregation of TDP43.

Pyridostatin (PDS), a small molecule that binds DNA and RNA G4s, and carboxypyridostatin (cPDS), an analog of PDS that specifically binds rG4s, were employed to test the effects of targeting G4s on TDP43 aggregation in cells[27,38–40]. We pretreated HEK293T-TDP43-YFP cells with 10 μM cPDS or 10 μM PDS for 8 h prior to introducing sodium arsenite. In the presence of either molecule, TDP43 aggregation

was significantly reduced; instead of puncta formation, diffuse TDP43-YFP signal was primarily observed within the nucleus (*Figure 2a,b*). To ensure this wasn't a product of the stable over-expression tag, TDP43-tdTomato was transiently transfected into HEK293T cells and similar results were seen with PDS and cPDS treatments (*Figure 2c*). Together, these results show that adding rG4 binders dramatically reduces TDP43 aggregation in HEK293T cells induced under conditions of oxidative stress.

Although arsenite stress is commonly used to test intracellular aggregation[36,37], we wanted to confirm whether the effects of the rG4 binding molecules were consistent with another type of protein stress. As a second stress model, we utilized proteasomal inhibition by the addition of MG132[41,42]. While robust aggregation of TDP43 formed in the nuclei of MG132 treated cells, cPDS and PDS treated cells retained a diffuse nuclear TDP43 distribution similar to that observed in control HEK293T cells (*Figure 2d,e*).

rG4 binders significantly inhibit the cytosolic redistribution and aggregation of overexpressed TDP43 in differentiated motor neuron-like NSC34 cells

To test the efficacy of these ligands in a more physiologically relevant system, we expanded these experiments to motor neuron-like NSC-34 cells. Differentiated NSC-34 cells overexpressing WT TDP43-tdTomato showed consistent nuclear localization of TDP43 under control conditions. However, when exposed to either oxidative or proteasomal stress, TDP43 exited the nucleus and formed cytoplasmic aggregates (*Figure 3a,b)*. Similar to results observed in the HEK293T cell model, preincubation of NSC-34 cells with either cPDS or PDS significantly inhibited the nuclear export of TDP43 induced by either sodium arsenite or MG132, resulting in a diffuse TDP43 signal remaining largely within the nucleus (*Figure 3c*).

To determine the effect of the rG4 binders on cell death when TDP43 is overexpressed in the NSC-34 cells, cell viability was quantified using a standard MTT assay. Without TDP43 overexpression, the cells showed little loss of viability in the presence or absence of proteasomal stress or rG4 binders (*Supplementary Figure 8a*). However, when TDP43 was overexpressed, cell death increased substantially, especially under proteasomal stress. Adding the rG4 binder cPDS resulted in a significant preservation of cell viability. Addition of PDS showed smaller, non-significant changes in viability, suggesting a potentially larger role of rG4s than G4s in stabilizing TDP43 (*Figure 3d*).

G-quadruplexes localize to TDP43 aggregates under induced cellular stress

Mechanistically, the ability for G4 binders to affect TDP43 aggregation is most plausible if both TDP43 and G4s co-localize in the described cell models. To test whether this was the case, we used an

immunostaining assay for RNA G4s using a BG4 antibody[43,44] in NSC-34 cells. The staining revealed that rG4s co-localize with TDP43 aggregates after oxidative stress or proteasome inhibition (*Figure 4)*. This co-localization is consistent with the direct modulation of TDP43 aggregation by G4s as observed *in vitro*, and the effects of the G4 binders observed here.

DISCUSSION

In this study, we examined the ability of rG4s to modulate the aggregation and toxicity of TDP43. *In vitro* experiments showed that G4s prevented the aggregation of TDP43. Experiments in yeast showed that exogenously added G4s could affect the level of TDP43 accumulation before cell death. Experiments in HEK293T cells demonstrated that the addition of rG4-binding molecules could resolve TDP43 aggregates. Finally, experiments in motor neuron-like NSC-34 cells showed that rG4s colocalized to TDP43 aggregates, and that the addition rG4 binding molecules both ameliorated aggregation and rescued viability from both oxidative and proteasomal stress. Together, these results suggest that modulating rG4s may be a novel therapeutic approach for diseases involving TDP43 mislocalization and aggregation.

cPDS is likely to bind rG4s of differing structures with differing affinities. Therefore, our analysis here is a simplification of what is a complex mixture of rG4 structures that are differently affected by the binding molecule. While in some cases, these molecules stabilize rG4 formation[27,38–40], this effect is likely structure-dependent. It is notable that cPDS was more effective at rescuing cytotoxicity than PDS, suggesting that the primary modulation here was of rG4s and not G4s.

Similarly, there are several different possibilities for the mechanism by which PDS and cPDS affect TDP43. It may be the case that they affect the structural pool of rG4s. As rG4s of parallel and anti-parallel topology have vastly different effects on aggregation[29,45], the PDS and cPDS could be shifting the population of the rG4 structures in a favorable manner. However, given the chemical similarity of these compounds to rG4s, it is possible that they are also to some degree binding TDP43 directly using the rG4 binding sites. Similarly, it is possible that the PDS and cPDS are preventing certain deleterious rG4 binding to TDP43 by binding to the rG4s. Because the population of differing structural rG4s topologies in the cell is, to our knowledge, completely unknown, it is difficult to determine which of these factors are most dominant in cells.

Overall, the results here demonstrate proof-of-principle results that modulating rG4 populations is a powerful way to modulate TDP43 aggregation and toxicity. As TDP43 is found to aggregate in multiple diseases[1–3,6–12,15,16], this could be a promising avenue for further therapeutic study, especially as rG4s are specifically targetable with small molecules. Of note, TDP43 is not the only disease-related protein that

binds to G4s, and other neurodegenerative disease aggregation proteins bind G4s as well[30], suggesting that this strategy could be effective in modulating the aggregation of proteins in many diseases.

STAR Methods:

REAGENT or RESOURCE	SOURCE	IDENTIFIER
Antibodies		
ChAT	Thermo	PA5-29653
TDP43	ProteinTech	10782-2-AP
AF647, ms	Thermo	A32728
AF647, rb	Thermo	A32795
anti-Flag	Cell Signaling Technologies	#2368
BG4	Millipore-Sigma	MABE917
Bacterial and virus strains		
DH5α *E. coli*		
BL21 *E. coli*		
Biological samples		
Chemicals, peptides, and recombinant proteins		
Human WT TDP43	AddGene	27458
RRM mut (5F->L)	AddGene	84914
LIC vector pET HisX6 eGFP TEV	AddGene	29663
pDonr221	GateWay yeast kit	
425 Gal __ DsRED	GateWay yeast kit	
425 Gal eGFP ___	GateWay yeast kit	
pcDNA3.2-TDP43-YFP	Addgene	84911
wtTDP43tdTomatoHA	Addgene	28205
pcDNA-YFP	Addgene	13033
NaAsO2	Sigma-Aldrich	S7400
MG132	Sigma-Aldrich	M7449
cPDS	MedChemExpress	HY-112680A
PDS	APExBIO	A3742
Critical commercial assays		

Deposited data		
Experimental models: Cell lines		
HEK293T-TDP43-YFP		
HEK293T-TDP43-tdTomato		
NSC34-TDP43-YFP		
NSC34-TDP43-tdTomato		
Experimental models: Organisms/strains		
BY4741 WT *S. cerevisiae*	Dharmacon	YSC1048
BY4741 deltaDBR1 *S. cerevisiae*	Dharmacon	YKL149c
Oligonucleotides		
5’ TTTAAGAAGGAGATATAGTTCGTGAGCAAGGGCGAGGAG 3’;	IDT	LIC Fwd, DNA
5’ GGATTGGAAGTAGAGGTTCTCCATTCCCCAGCCAGAAGA 3’	IDT	LIC Rev, DNA
5’ Cy5- GUGUAUUGAUUG 3’	IDT	AUG12, RNA
5’ Cy5- GUGUGUGUGUGU 3’	IDT	GU12, RNA
5’ GGGAGGCGTGGCCTGGGCGGGACTGGGG -6FAM 3’	IDT	LTRIII-6FAM, DNA
5’ TGTCGGGCGGGGAGGGGGGG -6FAM 3’	IDT	seq576-6FAM, DNA
5’ CGACATATGATAGGTGGACGATGG 3’	IDT	D169G Fwd, DNA
5’ CTGTGACATTACTTTCACTTGTGTTTCATATTCC 3’	IDT	D169G Rev, DNA
5’ CGGACCATTTGTACAAGAAAGCTGGGTACATTCCCCAGCCAGAAGACTAGAATCC 3’	IDT	attB1_NTD Fwd, DNA
5’ GCGGACAAGTTTGTACAAAAAGCAGGCTTCATGTCTGAATATATTCGG 3’	IDT	attB2_CTD Rev, DNA
Recombinant DNA		
Software and algorithms		
R	r-project.org	Version 4.3.2
FIJI	ImageJ	Version 1.54i
MatLab	MathWorks	R2023b

Other		

Resource availability

All data is available from the authors via emailing lead contact Scott Horowitz at scott.horowitz@du.edu

Cloning

A variety of cloning techniques for recombinant protein expression by *E. coli* and *S. cerevisiae* were used to purify protein for the use of *in vitro* assays and to express hTDP-43 in a model organism for *in vivo* assays.

Ligation Independent Cloning (LIC)

Human WT TDP43 (AddGene #27458), and RRM mut (5F → L) (AddGene #84914) open reading frames (ORFs) were cloned into the LIC vector pET HisX6 eGFP TEV cloning vector from AddGene (AddGene #29663) using QB Berkley LIC protocol with primers designed using the tool from QB3 MacroLab (Fwd: 5' TTTAAGAAGGAGATATAGTTCGTGAGCAAGGGCGAGGAG 3'; Rv: 5' GGATTGGAAGTAGAGGTTCTCCATTCCCCAGCCAGAAGA 3'). The primers were used to amplify the ORFs via polymerase chain reaction (PCR), and the LIC vector was digested with SspI restriction enzyme. The synthesized plasmid was then transformed into DH5α *Escherichia coli* before being isolated from 10 mL, single colony cultures, using a Genesee Miniprep kit, and sent for sequencing at Quintara Bio, and ultimately transformed into BL21.

Site-Directed Mutagenesis (SDM, QuickChange)

The point mutation D169G was generated using the New England Biolabs Q5® Site Directed Mutagenesis Kit (Fwd: 5' CGACATATGATAGGTGGACGATGG 3'; Rv: 5' CTGTGACATTACTTTCACTTGTGTTTCATATTCC 3'*)*. Synthesized plasmid was then transformed into DH5α *E. coli* for sequencing at Quintara Bio, and ultimately transformed into BL21 for expression and subsequent purification.

Gateway Cloning

The TDP43 sequences used were lifted using PCR with primers that included attB sites for compatibility with pDonr221 (Fwd: 5' CGGACCATTTGTACAAGAAAGCTGGGTACATTCCCCAGCCAGAAGACTAGAATCC 3'; Rv 5' GCGGACAAGTTTGTACAAAAAGCAGGCTTCATGTCTGAATATATTCGG 3') Yeast expression vectors were created using the Gateway® Cloning system and its included protocols[46–48]. The plasmid selected was a high copy, leucine auxotrophy, galactose inducible, C-terminal DsRED tagged one, after first being cloned, from a gBlock or PCR product, into a Gateway® Cloning entry vector, pDonr221.

Yeast cloning, plasmid

BY4741 WT yeast obtained from Dharmacon were grown to an approximate OD_{600} of 0.35, 250 μL were pelleted, rinsed with MBG H2O, briefly suspended in 100 mM LiOAc, before being pelleted and resuspended in 50 μL MBG H2O. 1 μg desired plasmid was then added to the yeast and allowed to incubate for 5 minutes before the addition of 10 μL sheared salmon DNA. 500 μL PLATE (40% PEG-3350, 100 mM LiOAc, 10 mM Tris pH 7.5, 1 mM EDTA) was then added. Samples were vortexed and allowed to incubate at 42°C for 35 minutes, then plated on selection media.

Protein purifications

The proteins used in these experiments were purified from recombinant DNA expressed by *E. coli* using affinity columns. Buffers, conditions, and purification and growth processes are detailed below for each of the experimentally used proteins.

eGFP-TDP-43 recombinant expression and purification of native protein

Cultures grown from a single colony of BL21 bacteria containing the plasmid for the desired construct were incubated at 37°C to an OD_{600} of approximately 0.4 before being induced with 1 mM IPTG for 6 h at 20°C. Cultures were then pelleted at 4°C at 8000 rpm for 30 minutes before decanting the media and resuspending the pellets in approximately 60 mL lysis buffer (40 mM HEPES, 300 mM NaCl, 1 mM $MgCl_2$, 50 mM Imidazole, 5 mM βMe, 10% glycerol), DNase (20 μg/μL), CHAPS (1%), and Egg White Lysozyme (0.25 mg/mL) were added and the resulting suspension was stirred at 4°C for 1 hour. After pelleting at 4°C at 31000 RCF for 75 minutes, the supernatant was filtered using a 0.22 μM Genesee bottle top filter before being loaded onto an 8 mL Biorad nickel immobilized metal affinity column (IMAC) column in an NGC

System from Biorad. The column was equilibrated in the lysis buffer and after loading the lysate by sample pump, 5 column volumes of lysis buffer were run over the column, followed by a gradient to 100% elution buffer (40 mM HEPES, 300 mM NaCl, 1 mM $MgCl_2$, 500 mM Imidazole, 5 mM βMe, 10% glycerol) over 3 column volumes. Samples were collected from the fractions that corresponded to a peak at 280 nm which occurred between 50-70% elution buffer. Collected fractions were pooled, filtered, and run on a GE Life Sciences Superdex 200 16/600 SEC with SEC buffer (40 mM HEPES, 300 mM NaCl, 5 mM DTT, 10% Glycerol). Purified fractions were pooled and then either used immediately or flash frozen and stored at -80°C for later use.

Analysis by Size exclusion chromatography

Samples were run on a GE Life Sciences Superdex 200 16/600 SEC with SEC buffer (40 mM HEPES, 300 mM NaCl, 5 mM DTT, 10% Glycerol). Commercial sizing standards (https://www.bio-rad.com/en-us/sku/1511901-gel-filtration-standard?ID=1511901) were run as well.

Turbidity

The protein was loaded into a 96 well plate and the turbidity of the sample at 395 nm and 600 nm was monitored over time at room temperature with no shaking. 4 measurements were taken of each well, and averaged, every 2 minutes for 90-1200 minutes.

Yeast viability assays

TDP43 and control protein expressing yeast were examined for yeast vitality, by serial dilution on an agar plate. G-quadruplex LTRIII -6FAM was observed to be taken into the cytoplasm of the yeast when added directly to the media, as was fluoresceine (*Supplementary figure 3*). The working concentration of the oligos as drugs for cell sorter experiments was determined to be 10 μM for the low copy, galactose inducible TDP-43-DsRED yeast expression plasmid (*Figure 1d,e, Supplementary Figure 5*).

Spotting assay

BY4741 WT yeast containing the Gateway plasmid 425 Gal ___ DsRED with the various point mutants and other listed proteins were allowed to grow in 2% glucose selection media (-Leu) to an OD_{600} between 0.1 and 0.3. ODs were measured in triplicate and averaged before being diluted to 0.01 and 7 serial dilutions of 1 to 8 were done. This was spotted onto 2% glucose -Leu agar plates and 4% galactose -Leu agar plates. Plates were imaged every 12 h of growth at 30°C for 3 days.

Cell sorter analysis

Cell sorting of BY4741 WT 415 Gal TDP-43 DsRED live cell imaging. Low copy plasmid is 1 copy (CEN)[48,49] high copy is 40-60 copies (2μ)[46,48]. AUG12 and GT12 are known TDP-43 binders. Cells were grown to an OD_{600} of 0.3 in SD 2% glucose media, then induced with 4% galactose –His media for 8hrs, then 1 μM LTRIII-3' 6FAM (5' GGGAGGCGTGGCCTGGGCGGGACTGGGG-6FAM 3'), seq576-6FAM (5' TGTCGGGCGGGGAGGGGGGG 3'), AUG12-3' 6FAM (5' GUGUGAAUGAAU-6FAM 3'), GT12-6FAM (5' GTGTGTGTGTGT-6FAM 3'), or fluorescein was added and cells were allowed to grow for 16 h. Cells are pelleted and washed twice with PBS (137 mM NaCl, 2.7 mM KCl, 4.3 mM Na_2HPO_4,1.47 mM KH_2PO_4, pH = 7.4), and then resuspended in PBS, stained with DRAQ7 as a nuclear death stain. Excess DRAQ7 is then removed by washing cells twice with PBS before being resuspended in PBS. An SH800 Sony Cell Sorter is then calibrated using a mix of 3 μm and 10 μm nanobeads (Sony Automatic Setup Beads LE-B3001), before sorting 100,000 cells for the following distributions: DsRED (PE-A) vs. Back scattering**,** DRAQ7 (7AAD) vs. back scattering, 6FAM (CSFE) vs. back scattering, 6FAM vs. DRAQ7, DsRED vs. DRAQ7.

Spinning disc confocal microscopy of yeast

BY4741 WT yeast containing the Gateway plasmid 425 Gal ___ DsRED with the various point mutants and other listed proteins. The yeast were grown to an OD_{600} of 0.1 in 2% Glucose selection media (-Leu) before being pelleted, resuspended in the same volume 4% Galactose selection media, and allowed to continue to grow for 7.5 h. The yeast were then pelleted, washed with PBS twice, resuspended in PBS, and plated for imaging with an Olympus FV300 spinning disc confocal. Images are processed by using FIJI and are de-speckled and smoothed using the included software of FIJI. Z stacks were averaged and combined for the DsRED channel using the program included in FIJI.

Cell culture

Human embryonic kidney 293T (HEK293T) cells were grown in culture medium (High Glucose DMEM (Hy-Clone), 10% HI FBS (Gibco), 1% L-glutamine (Gibco), 1% Pen/Strep (Gibco)) on 10 cm tissue culture dishes and incubated at 37°C and 5% CO_2. For all experiments, cells between passages 5 and 20 were used to maintain consistency.

Immortalized neuroblastoma x spinal cord cells (NSC-34; kindly provided by Barbera Corneo, Columbia University) were cultured in medium containing high glucose DMEM, 10% FBS, and 1% pen/strep, in 6-well tissue culture plates (CellTreat) and incubated at 37°C and 5% CO_2.

Mammalian TDP43 stable and transient overexpression transfection

pcDNA3.2 TDP43 YFP (Addgene #84911) was graciously provided by the Aaron Gitler Lab, wtTDP43tdTOMATOHA (Addgene #28205) was graciously provided by the Zuoshang Xu Lab, and pcDNA3-YFP (Addgene #13033) was graciously provided by the Doug Golenbock Lab. These plasmids were transformed into DH5α *E. coli* before being isolated from 5 mL, single colony cultures, using an Omega Bio-Tek Miniprep Kit. These plasmids were transfected into HEK293T and NSC34 cell lines with Lipofectamine 2000 (Invitrogen, 11668027) 24 h prior to stable selection or transient experimentation, respectively.

HEK293T cells were seeded in a 24-well tissue culture plate (CellTreat) at 1.5 x10^5 and incubated overnight. Lipofectamine 2000 was used per manufacturer's protocol with 500 ng of pcDNA3.2 TDP-43 YFP[36] added per well. Cells were split the following day into single colonies and cultured in 500 µg/mL G418 to select for YFP positive cells. TDP43-YFP cells were passed at 80% confluency, seeded at 1 x 10^6 HEK293T cells per passage, and maintained in 200 µg/mL G418. wtTDP43-tdTomatoHA[50] was transiently transfected as described above.

NSC34 Cell Culture Differentiation

For immunocytochemistry assays, NSC-34 cells were seeded on 0.5 mg/mL Poly-D-Lysine treated #1.5 cover glass in 24 well plates (MatTek) at 75,000 cells/mL. For viability (MTT) assays, NSC-34 cells were seeded at 150,000 cells/mL in 6 well plates (CellTreat). Maintenance media (DMEM, 10% FBS, 1% P/S) was swapped 24 h after seeding to differentiation media containing: 1:1 DMEM/F-12 (Ham), 0.5% FBS, 1% modified Eagle's medium nonessential amino acids (NEAA), 1% P/S, and 10 µM all-trans retinoic acid (atRA), and differentiation media was switched every 48 h for 5 days. These cells were cultured and transfected with the wtTDP43tdTOMATOHA plasmid and differentiated with culture media containing 10 µM retinoic acid for 96 h before experiments were performed. Optimal differentiation was verified by immunocytochemistry for ChAT (Invitrogen, PA5-29653) antibody staining under normal, oxidative, and proteasomal stress conditions.

Administration of G4 Binders

To test neuroprotective effects of G4 binders, Pyridostatin and Carboxypyridostatin were incubated prior to perturbations for 8 h at 37°C, then fixed and imaged. Cell models were prepared as previously stated. HEK293T models were treated with 10μM of PDS and cPDS, while NSC34 models were treated with 5 μM. 0.1% and 0.05% DMSO were used as vehicle controls for G4 binder delivery.

Mammalian Cell TDP43 Aggregation

To induce TDP43 aggregation, Sodium Arsenite ($NaAsO_2$, Sigma-Aldrich, S7400) and MG132 (Sigma-Aldrich, M7449) were added to G4 binder pretreated and negative control prepared HEK293T and differentiated NSC34 cells.

For immunocytochemistry, in HEK293T models, $NaAsO_2$ and MG132 were added at 10 μM working concentrations and incubated at 37C for 8 h prior to fixation. In NSC34 models, $NaAsO_2$ and MG132 were added at 2.5 μM and 5 μM, respectively, and incubated at 37°C for 8 h prior to fixation.

For cell viability (MTT) assays, aggregation agents were incubated at 37°C for 36 h and concentrations stated above.

MTT Tetrazolium Cell Viability Assay

The MTT (3-(4,5-dimethylthiazol-2-yl)-2,5-diphenltetrazolium bromide) tetrazolium reduction assay was used to quantify viability of NSC34 cell lines. Thiazolyl Blue Tetrazolium Bromide (MTT Powder) (Sigma-Aldrich, M2128) reagent was prepared dissolving MTT in Dulbecco's Phosphate Buffer Solution (DPBS), pH = 7.4, to 5 mg/mL, filtered. 200 μL of reagent was added to differentiated NSC34 plates to a final concentration of 0.45 mg/mL and incubated at 37°C for 3 h. 2 mL of DMSO was added to dissolve formazan crystals and agitated on plate shaker for 10 min to ensure complete solubilization. Wells were aliquoted into black wall 96 well plate and absorbance were recorded at 570 nm on a Tecan Infinite M200Pro.

Immunocytochemistry and Confocal Imaging

Cells and test compounds were prepared as previously stated and were fixed in 4% Paraformaldehyde (PFA) for 20 minutes, permeabilized with solution of 0.1% Triton X-100 and 1x DPBS for 10 min, then blocked with blocking buffer solution (0.2% gelatin, 0.5% Triton X-100, DPBS, pH=7.4) for 1 hour. Primary and secondary antibodies were diluted in blocking buffer and incubated on coverslips away from light at 25°C for 1 hour, respectively (anti-TDP43 (1:50), Rb, ProteinTech, 10782-2-AP; anti-ChAT (1:200), Rb, Invitrogen, PA5-29653; anti-BG4 (1:50), Ms, Millipore-Sigma, MABE917; anti-Flag (MA4) (1:50), Ms, Cell Signaling Tech, #2368; Goat anti-mouse IgG (H+L) Highly Cross-Adsorbed Alexa-Fluor Plus 647 (1:1000), Invitrogen, A32728; Donkey anti-rabbit IgG (H+L) Highly Cross-Adsorbed Alexa-Fluor Plus 647 (1:1000), Invitrogen, A32795). Nuclei were labeled by the addition of 1 ug/mL Hoechst stain (33342,

Invitrogen, #62249), incubated away from light for 10 minutes. Coverslips were imaged via confocal microscopy (Olympus FV3000).

Statistical Analysis

Experiments were performed using duplicate or triplicate replicates for all biologic and *in vitro* samples. Error bars represent the mean +/- the standard error. Statistical analyses were performed using one-way analysis of variance (ANOVA) in R and Matlab. Differences between treatment groups were considered to be statistically significant at a p value of $p < 0.05$.

Acknowledgements

This work was funded by a CDMRP ALSRP grant (W81XWH-22-1-0218). The authors would like to thank David Robinson and Nicole Toro for aid in some of the molecular cloning, and Yan Qin and Anna Dischler for assistance with time lapse microscopy.

Declaration of Interests: No conflicts of interest

References

1. Klim, J., Pintacuda, G., Nash, L., Guerra San Juan, I., and Eggan, K. (2021). Connecting TDP-43 Pathology with Neuropathy. Trends Neurosci *44*, 424–440. 10.1016/j.tins.2021.02.008.
2. François-Moutal, L., Felemban, R., Scott, D., Sayegh, M., Miranda, V., Perez-Miller, S., Khanna, R., Gokhale, V., Zarnescu, D., and Khanna, M. (2019). Small Molecule Targeting TDP-43's RNA Recognition Motifs Reduces Locomotor Defects in a Drosophila Model of Amyotrophic Lateral Sclerosis (ALS). ACS Chem Biol *14*, 2006–2013. 10.1021/acschembio.9b00481.
3. François-Moutal, L., Perez-Miller, S., Scott, D., Miranda, V., Mollasalehi, N., and Khanna, M. (2019). Structural Insights Into TDP-43 and Effects of Post-translational Modifications. Front Mol Neurosci *12*. 10.3389/fnmol.2019.00301.
4. Lagier-Tourenne, C., Polymenidou, M., and Cleveland, D. (2010). TDP-43 and FUS/TLS: emerging roles in RNA processing and neurodegeneration. Hum Mol Genet *19*, R46–R64. 10.1093/hmg/ddq137.
5. Ratti, A., and Buratti, E. (2016). Physiological functions and pathobiology of TDP-43 and FUS/TLS proteins. J Neurochem *38*, 95–111. 10.1111/jnc.13625.
6. Ayala, Y., Zago, P., D'Ambrogio, A., Xu, Y.-F., Petrucelli, L., Buratti, E., and Baralle, F. (2008). Structural determinants of the cellular localization and shuttling of TDP-43. J Cell Sci *121*, 3778–3785. 10.1242/jcs.038950.
7. Jiang, L., Xue, W., Hong, J., Zhang, J., Li, M., Yu, S., He, J., and Hu, H. (2017). The N-terminal dimerization is required for TDP-43 splicing activity. Sci Rep *7*, 6196. 10.1038/s41598-017-06263-3.

8. Johnson, B., McCaffery, J., Lindquist, S., and Gitler, A. (2008). A yeast TDP-43 proteinopathy model: Exploring the molecular determinants of TDP-43 aggregation and cellular toxicity. Proc Natl Acad Sci USA *105*, 6439–6444. 10.1073/pnas.0802082105.
9. Aguzzi, A., and Calella, A. (2009). Prions: protein aggregation and infectious diseases. Physiol Rev. *89*, 1105–1152. 10.1152/physrev.00006.2009.
10. De Baets, G., Van Doorn, L., Rousseau, F., and Schymkowitz, J. (2015). Increased Aggregation Is More Frequently Associated to Human Disease-Associated Mutations Than to Neutral Polymorphisms. PLoS Comput Biol *11*, e1004374. 10.1371/journal.pcbi.1004374.
11. Du, K., Karp, P., Ackerley, C., Zabner, J., Keshavjee, S., Cutz, E., and Yeger, H. (2015). Aggregates of mutant CFTR fragments in airway epithelial cells of CF lungs: new pathologic observations. J Cyst Fibros *14*, 182–193. 10.1016/j.jcf.2014.09.012.
12. Kumar, S., Thangakani, A., Nagarajan, R., Singh, S., Velmurugan, D., and Gromiha, M. (2016). Autoimmune Responses to Soluble Aggregates of Amyloidogenic Proteins Involved in Neurodegenerative Diseases: Overlapping Aggregation Prone and Autoimmunogenic regions. Sci Rep *6*. 10.1038/srep22258.
13. Foster, A., Flynn, L., Cluning, C., Cheng, F., Davidson, J., Lee, A., Polain, N., Mejzini, R., Farrawell, N., Yerbury, J., et al. (2021). p62 overexpression induces TDP-43 cytoplasmic mislocalisation, aggregation and cleavage and neuronal death. Sci Rep *11*, 11474. 10.1038/s41598-021-90822-2.
14. Morimoto, R., and Cuervo, A. (2009). Protein homeostasis and aging: taking care of proteins from the cradle to the grave. J Gerontol A Biol Sci Med Sci *64*, 167–170. 10.1093/gerona/gln071.
15. Ross, C., and Poirier, M. (2004). Protein aggregation and neurodegenerative disease. Nat Med *10*, S10-7. 10.1038/nm1066.
16. Tomé, S., Tsaka, G., Ronisz, A., Ospitalieri, S., Gawor, K., Gomes, L., Otto, M., von Arnim, C., Van Damme, P., Van Den Bosch, L., et al. (2023). TDP-43 pathology is associated with increased tau burdens and seeding. Mol Neurodegener *18*. https://doi.org/10.1186/s13024-023-00653-0.
17. Wang. C, Duan, Y., Duan, G., Wang, Q., Zhang, K., Deng, X., Qian, B., Gu, J., Ma, Z., Zhang, S., et al. (2020). Stress Induces Dynamic, Cytotoxicity-Antagonizing TDP-43 Nuclear Bodies via Paraspeckle LncRNA NEAT1-Mediated Liquid-Liquid Phase Separation. Mol Cell *79*, 443–458. 10.1016/j.molcel.2020.06.019.
18. Asakawa, K., Handa, H., and Kawakami, K. (2021). Multi-phaseted problems of TDP-43 in selective neuronal vulnerability in ALS. Cell Mol Life Sci *78*, 4453–4465. 10.1007/s00018-021-03792-z.
19. Matsukawa, K., Kukharsky, M., Park, S., Park, S., Watanabe, N., Iwatsubo, T., Hashimoto, T., Liebman, S., and Shelkovnikova, T. (2019). Long non-coding RNA NEAT1_1 ameliorates TDP-43 toxicity in in vivo models of TDP-43 proteinopathy. RNA Biol *18*, 1546–1554. 10.1080/15476286.2020.1860580.
20. Qin, H., Lim, L., Wei, Y., and Song, J. (2014). TDP-43 N terminus encodes a novel ubiquitin-like fold and its unfolded form in equilibrium that can be shifted by binding to ssDNA. Proc Natl Acad Sci U S A. *111*, 18619–18624. 10.1073/pnas.1413994112.

21. Mann, J., Gleixner, A., Mauna, J., Gomes, E., DeChellis-Marks, M., Needham, P., Copley, K., Hurtle, B., Portz, B., Pyles, N., et al. (2019). RNA Binding Antagonizes Neurotoxic Phase Transitions of TDP-43. Neuron *102*, 321–338. 10.1016/j.neuron.2019.01.048.
22. Lukavsky, P., Daujotyte, D., Tollervey, J., Ule, J., Stuani, C., Buratti, E., Baralle, F., Damberger, F., and Allain, F. (2013). Molecular basis of UG-rich RNA recognition by the human splicing factor TDP-43. Nat Struct Mol Biol *20*, 1443–1449. 10.1038/nsmb.2698.
23. Fujimoto, A., Kinjo, M., and Kitamura, A. (2022). Short repeat RNA reduces cytotoxicity by preventing the aggregation of TDP-43 and its 25 kDa carboxy-terminal fragment. Preprint at bioRxiv. https://doi.org/10.1101/2022.07.03.498631.
24. Ishiguro, A., and Ishihama, A. (2023). ALS-linked TDP-43 mutations interfere with the recruitment of RNA recognition motifs to G-quadruplex RNA. Sci Rep *13*, 5982. 10.1038/s41598-023-33172-5.
25. Ishiguro, A., Kimura, N., Watanabe, Y., Watanabe, S., and Ishihama, A. (2016). TDP-43 binds and transports G-quadruplex-containing mRNAs into neurites for local translation. Genes Cells *21*, 466–481. 10.1111/gtc.12352.
26. Ishiguro, A., Katayama, A., and Ishihama, A. (2021). Different recognition modes of G-quadruplex RNA between two ALS/FTLD-linked proteins TDP-43 and FUS. FESB Lettr *595*, 310–323. 10.1002/1873-3468.
27. Kharel, P., Fay, M., Manasova, E., Anderson, P., Kurkin, A., Guo, J., and Ivanov, P. (2023). Stress promotes RNA G-quadruplex folding in human cells. Nat Commun *14*. https://doi.org/10.1038/s41467-023-35811-x.
28. Asamitsu, S., Yabuki, Y., Matsuo, K., Kawasaki, M., Hirose, Y., Kashiwazaki, G., Chandran, A., Bando, T., Wang, D., Sugiyama, H., et al. (2023). RNA G-quadruplex organizes stress granule assembly through DNAPTP6 in neurons. Sci Adv *9*, 2035. 10.1126/sciadv.ade2035.
29. Begeman, A., Son, A., Litberg, T., Wroblewski, T., Gehring, T., Huizar Cabral, V., Bourne, J., Xuan, Z., and Horowitz, S. (2020). G-Quadruplexes act as sequence-dependent protein chaperones. EMBO Rep *21*, e49735. 10.15252/embr.201949735.
30. Guzman, B., Son, A., Litberg, T., Huang, Z., Dominguez, D., and Horowitz, S. (2023). Emerging roles for G-quadruplexes in proteostasis. FEBS J *21*, e49735. 10.15252/embr.201949735.
31. Son, A., Huizar Cabral, V., Huang, Z., Litberg, T., and Horowitz, S. (2023). G-quadruplexes rescuing protein folding. Proc Natl Acad Sci U S A. *20*, e2216308120. 10.1073/pnas.2216308120.
32. Armakola, M., Hart, M., and Gitler, A. (2011). TDP-43 toxicity in yeast. Methods *53*, 238–245. 10.1016/j.ymeth.2010.11.006.
33. Park, S., Hong, J., Arslan, F., Kanneganti, V., Patel, B., Tietsort, A., Tank, E., Li, X., Barmada, S., and Liebman, S. (2017). Overexpression of the essential Sis1 chaperone reduces TDP-43 effects on toxicity and proteolysis. PLoS Genet *13*, e1006805. 10.1371/journal.pgen.1006805.
34. Wall, M., Socolich, M., and Ranganathan, R. (2000). The structural basis for red fluorescence in the tetrameric GFP homolog DsRed. Nat Struct Biol *7*, 1133–1138. 10.1038/81992.

35. Chiang, C., Grauffel, C., Wu, L., Kuo, P., Doudeva, L., Lim, C., Shen, C., and Yuan, H. (2016). Structural analysis of disease-related TDP-43 D169G mutation: linking enhanced stability and caspase cleavage efficiency to protein accumulation. Sci Rep *6*. https://doi.org/10.1038/srep21581.
36. Elden, A., Kim, H., Hart, M., Chen-Plotkin, A., Johnson, B., Fang, X., Armakola, M., Geser, F., Greene, R., Lu, M., et al. (2010). Ataxin-2 intermediate-length polyglutamine expansions are associated with increased risk for ALS. Nature *466*, 1069–1075. 10.1038/nature09320.
37. Zhang, K., Daigle, J., Cunningham, K., Coyne, A., Ruan, K., Grima, J., Bowen, K., Wadhwa, H., Yang, P., Rigo, F., et al. (2018). Stress Granule Assembly Disrupts Nucleocytoplasmic Transport. Cell *173*, 958–971. 10.1016/j.cell.2018.03.025.
38. Figueiredo, J., Miranda, A., Lopes-Nunes, J., Carvalho, J., Alexandre, D., Valente, S., Mergny, J., and Cruz, C. (2021). Targeting nucleolin by RNA G-quadruplex-forming motif. Biochem Pharmacol *189*, 114418. 10.1016/j.bcp.2021.114418.
39. Rocca, R., Talarico, C., Moraca, F., Costa, G., Romeo, I., Ortuso, F., Alcaro, S., and Artese, A. (2017). Molecular recognition of a carboxy pyridostatin toward G-quadruplex structures: Why does it prefer RNA? . Chem Biol Drug Des *90*, 919–925. 10.1111/cbdd.13015.
40. Spiegel, J., Adhikari, S., and Balasubramanian, S. (2020). The Structure and Function of DNA G-Quadruplexes. Trends Chem *2*, 123–136. 10.1016/j.trechm.2019.07.002.
41. Scotter, E., Vance, C., Nishimura, A., Lee, Y., Chen, H., Urwin, H., Sardone, V., Mitchell, J., Rogelj, B., Rubinsztein, D., et al. (2014). Differential roles of the ubiquitin proteasome system and autophagy in the clearance of soluble and aggregated TDP-43 species. J Cell Sci *127*, 1263–1278. 10.1242/jcs.140087.
42. van Eersel, J., Ke, Y., Gladbach, A., Bi, M., Götz, J., and Kril, J. (2011). Cytoplasmic Accumulation and Aggregation of TDP-43 upon Proteasome Inhibition in Cultured Neurons. PLoS One *6*, e22850. 10.1371/journal.pone.0022850.
43. Biffi, G., Tannahill, D., McCafferty, J., and Balasubramanian, S. (2013). Quantitative visualization of DNA G-quadruplex structures in human cells. Nat Chem *5*, 182–186. 10.1038/nchem.1548.
44. Zhang, M., Liu, R., and Wang, F. (2019). Telomere and G-Quadruplex Colocalization Analysis by Immunofluorescence Fluorescence In Situ Hybridization (IF-FISH). Methods Mol Biol *1999*, 327–333. 10.1007/978-1-4939-9500-4_23.
45. Litberg, T., Sannapureddi, R., Huang, Z., Son, A., Sathyamoorthy, B., and Horowitz, S. (2023). Why are G-quadruplexes good at preventing protein aggregation? RNA Biol *20*, 495–509. 10.1080/15476286.2023.2228572.
46. Chan, K., Liu, Y., Ma, C., Jayaram, M., and Sau, S. (2013). The 2 micron plasmid of Saccharomyces cerevisiae: a miniaturized selfish genome with optimized functional competence. Plasmid *70*, 2–17. 10.1016/j.plasmid.2013.03.001.
47. Katzan, F. (2007). Gateway(®) recombinational cloning: a biological operating system. Expert Opin Drug Discov *2*, 571–589. 10.1517/17460441.2.4.571.
48. Alberti, S., Gitler, A., and Lindquist, S. (2007). A suite of Gateway cloning vectors for high-throughput genetic analysis in Saccharomyces cerevisiae. Yeast *24*, 913–919. 10.1002/yea.1502.

49. AddGene Plasmids 101: Yeast Vectors. http://blog.addgene.org/plasmids-101-yeast-vectors. http://blog.addgene.org/plasmids-101-yeast-vectors.
50. Yang, C., Tan, W., Whittle, C., Qiu, L., Cao, L., Akbarian, S., and Xu, Z. (2010). The C-terminal TDP-43 fragments have a high aggregation propensity and harm neurons by a dominant-negative mechanism. PLoS One *5*, e15878. 10.1371/journal.pone.0015878.

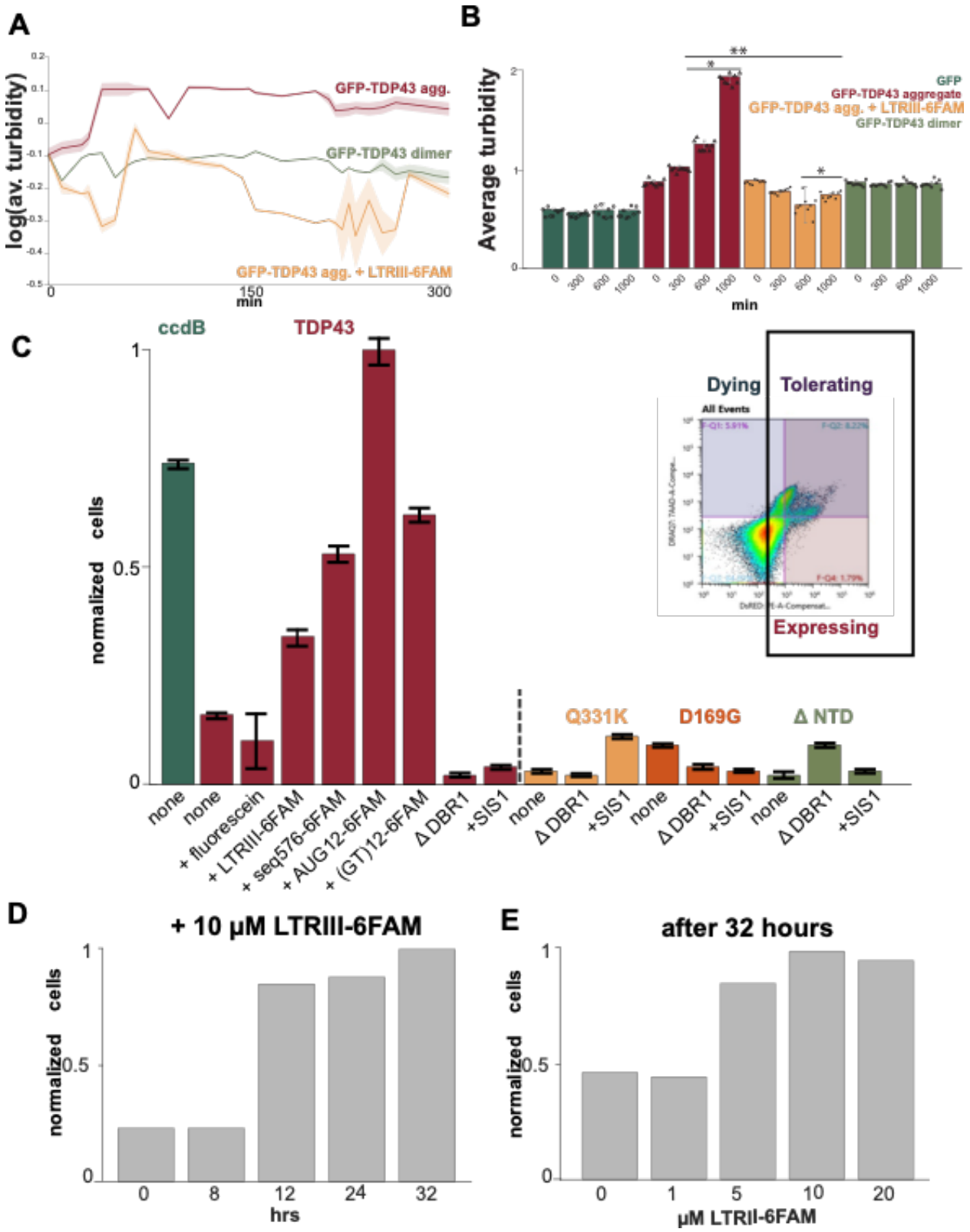

Figure 1. G4s modulate TDP43 aggregation *in vitro* and in yeast. A-B. The coincubation of eGFP-TDP43 with LTRIII-6FAM slows down the aggregation of the protein as measured by dynamic light

scattering and turbidity at 395 nm. 50 μM eGFP-TDP43 was co-incubated with 10 μM G4 in 40 mM HEPES pH 7.5, 300 mM NaCl, 1 mM $MgCl_2$, 10% glycerol, 5 mM DTT, for 8.5 h at RT and allowed to aggregate. eGFP-TDP43 protein aggregates and dimer, as separated by SEC. Each time point has three technical and three independent replicates. Error bars indicate standard error. A. Change in turbidity at OD_{395} over time. B. turbidity of the samples at 0, 300, 500, and 1000 minutes are included to show eGFP-TDP43 aggregate falling out of solution. One-way ANOVA with Tukey's comparison test were done where applicable. **p = 0.000001, *p = 0.00703. C-E. The treatment of TDP43-DsRED expressing yeast with nucleic acids results in an increase in the percent of cells tolerating and expressing the TDP43-DsRED. These are the normalized percent of yeast cells as quantified using a cell sorter to sort cells by DsRED intensity and DRAQ7 intensity. C. TDP43 and disease point mutants have diminished vitality when expressing TDP43-DsRED, which is rescued by the addition of 10 μM G4. Overexpression of SIS1 and deletion of DBR1 in yeast do not increase the levels of TDP43 in cells. Inset displays the gating and classification for all samples for 10 μM LTRIII-6FAM and TDP43-DsRED expressing yeast after 32 h of growth. D. A time course of the normalized % cells tolerating and expressing TDP43-DsRED co-incubated with 10 μM LTRIII-6FAM. E. A dosage curve of the normalized percent cells tolerating and expressing TDP43-DsRED with LTRIII-6FAM after 32 h. 100,000 cells/replicate used for all cytometry.

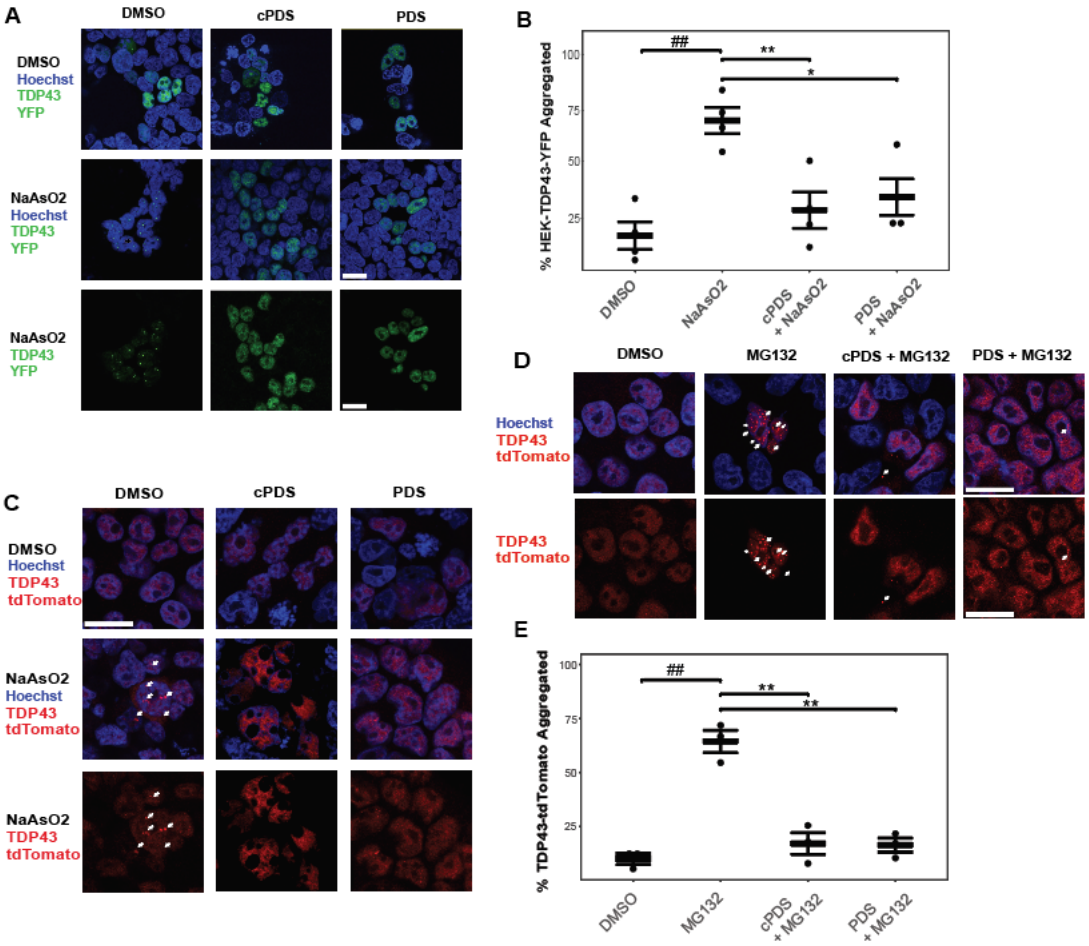

Figure 2. G4 Binders mitigate oxidative and proteasomal stress induced aggregation in HEK293T cells overexpressing TDP43. Nuclear stain Hoechst 33242 (blue) A**.** Stable overexpression HEK293T-TDP43-YFP (green) cells were treated with 10 µM PDS and cPDS, for 8 h prior to oxidative stress ($NaAsO_2$, 10 µM) Imaging: 60x, scale bar = 20 µm. B. Quantification of aggregated nuclear and cytoplasmic TDP43 were compared to transfected unaggregated nuclei; (Welch's two sample t-test, unpaired; ##, **, $p < 0.01$; *, $p < 0.05$), n = 4. C**.** Oxidative stress and G4 Binders assays were repeated in HEK293T cells with TDP43-tdTomato (red) transient transfection. D-E. HEK293T cells were subject to proteosome inhibitor MG132 (10 µM) for 8 h. Pretreatment with G4 binders (10 µM for 8 h) and proteosome stress were repeated and aggregates were quantified; (Welch's two sample t-test, unpaired; ##, **, $p < 0.01$) n=3.

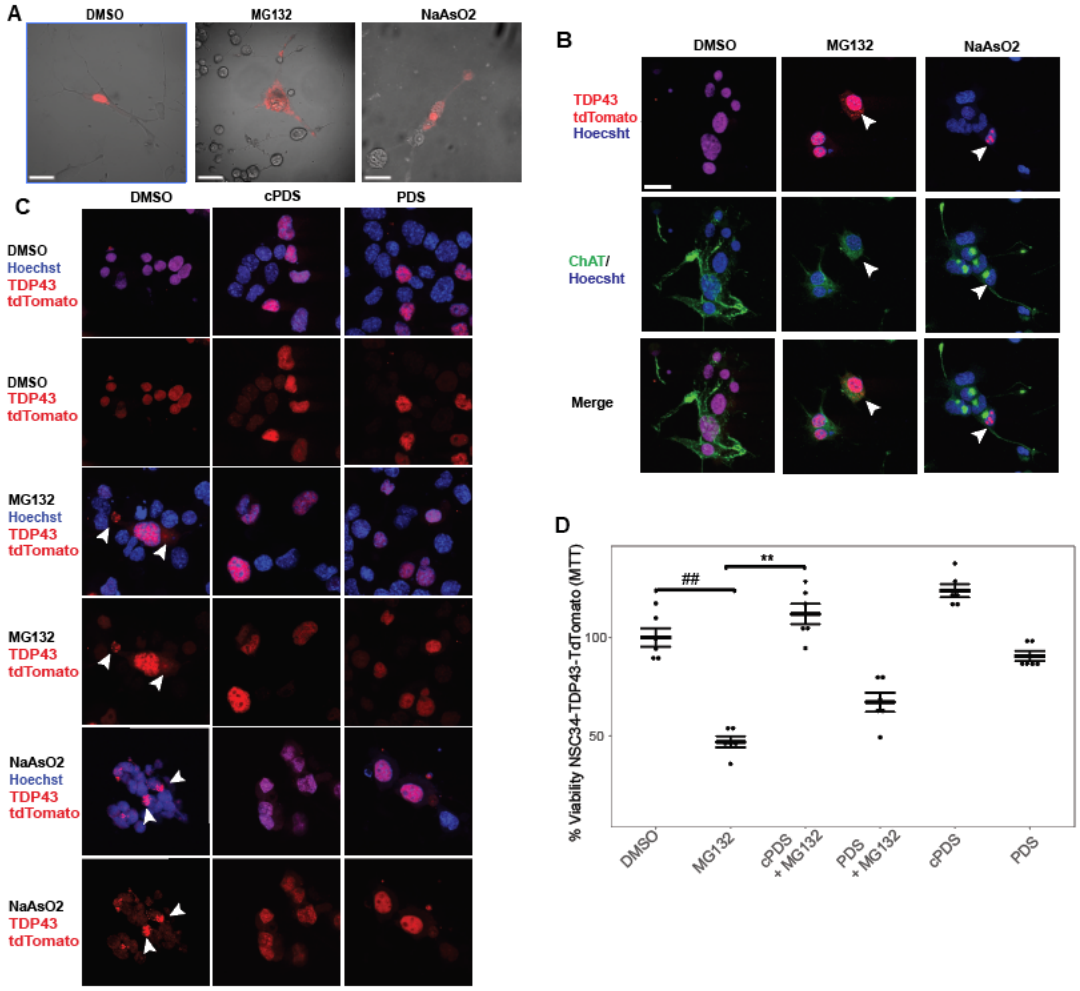

Figure 3. G4 Binders mitigate oxidative and proteasomal stress induced aggregation in TDP43 overexpressed NSC34 cells. A. NSC-34 cells transfected with TDP43-tdTomato differentiated for 96h in low serum media with 10 µM Retinoic Acid (R.A.). MG132 and $NaAsO_2$ induced cytosolic aggregation of TDP43 within 8h. B. Differentiation was confirmed with immunofluorescent anti-ChAT, ms Alexa-Fluor 647 (green), nuclear labeled Hoechst 33342 (blue), and cytosolic inclusions are formed within 8h of 5 µM $NaAsO_2$ and 5 µM MG132 stress. C. When treated with G4 binders, cytosolic aggregates are lessened in both stress conditions; n = 6**.** D. MTT data of NSC34-tdTomatoTDP43; in overexpression model, cell viability and survival significantly improved when pretreated with 5 µM cPDS and near significance in 5 µM PDS (Two-way ANOVA, Tukey's post-hoc test, unpaired; ##, **, $p < 0.01$) n = 6.

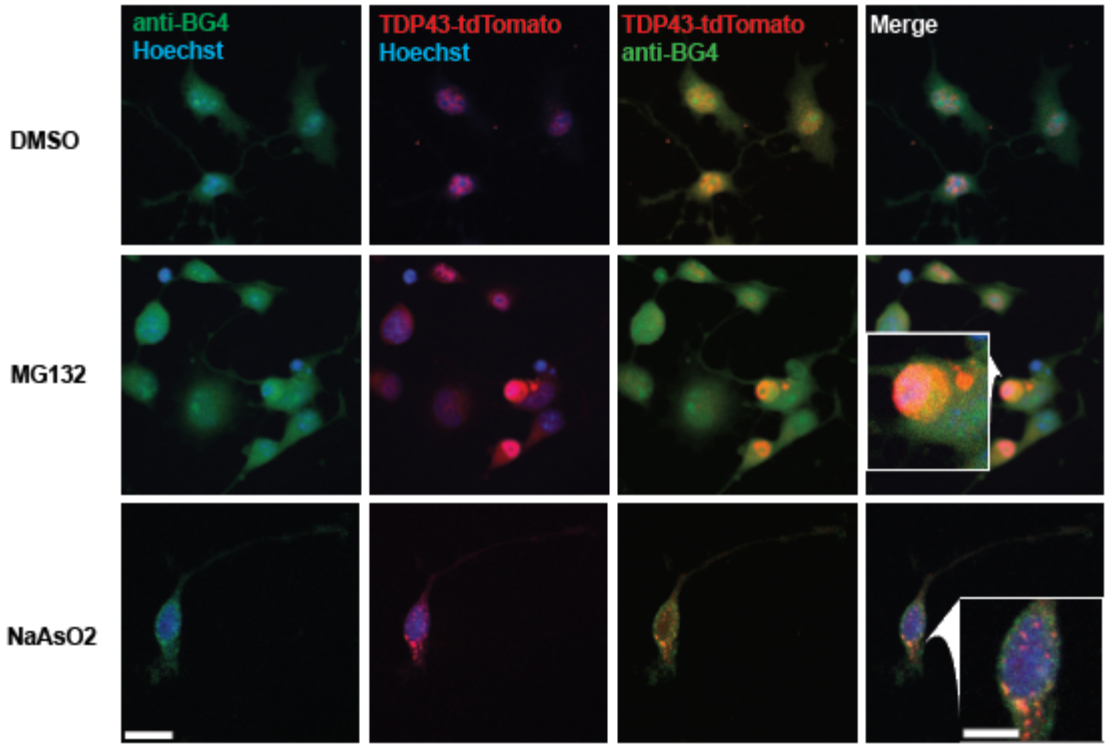

Figure 4. Immunocytochemistry NSC34 TDP43-tdTomato cells stained with anti-BG4 (1:50) suggested colocalization of RNA G-quadruplexes with aggregated TDP43 under oxidative and proteasomal stress conditions. Anti-BG4, rb Alexa-Fluor 647(green), stained for rG4s in NSC34 overexpressing TDP43-tdTomato. Scale bars, anti-BG4/Hoechst = 40 µm; inset = 20 µm.

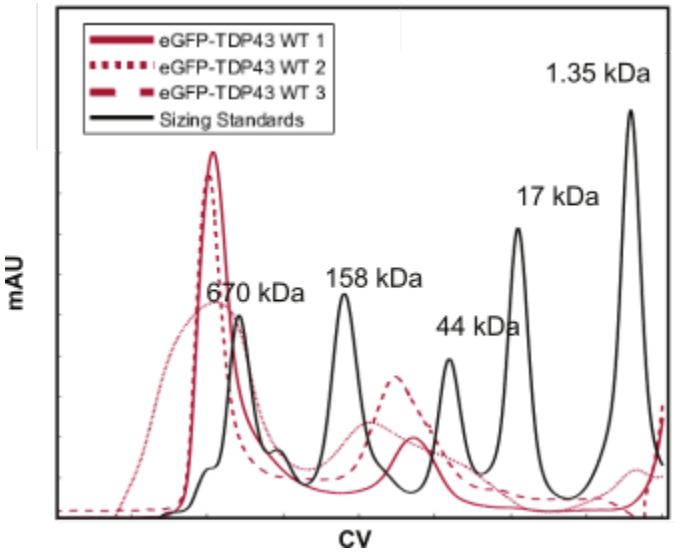

Supplementary Figure 1. Size exclusion chromatography was used to separate the aggregate eGFP-TDP43 and the dimeric eGFP-TDP43 in 40 mM HEPES pH = 7.5, 300 mM NaCl, 1 mM $MgCl_2$, 10% glycerol, in triplicate with BioRad sizing standards.

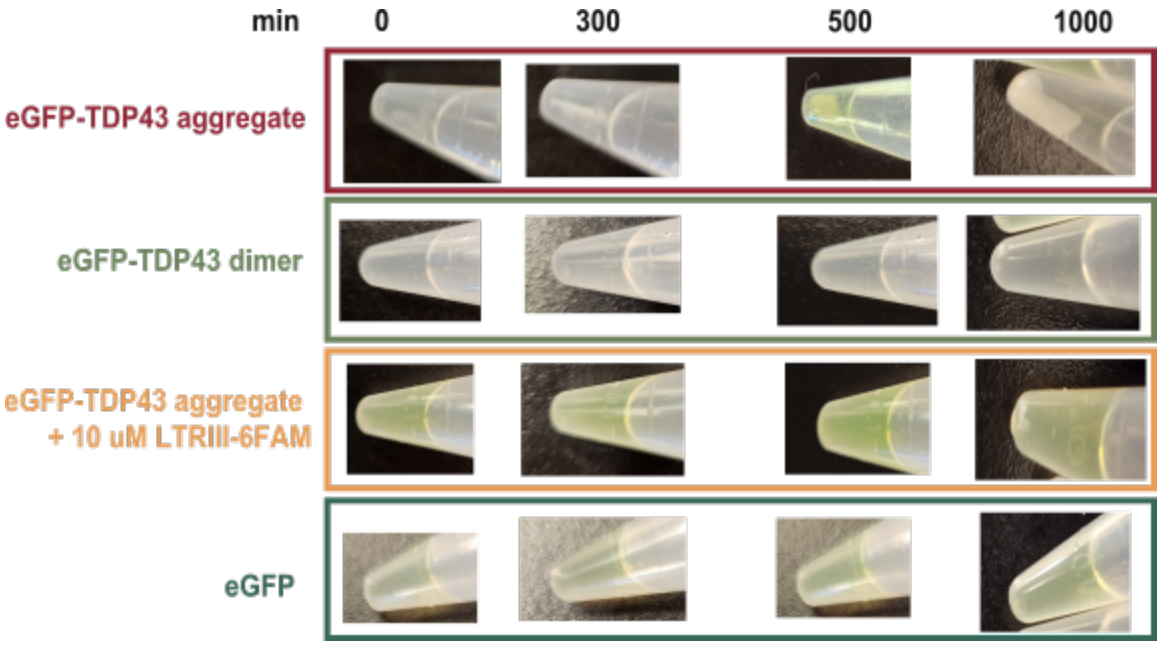

Supplementary Figure 2. As eGFP-TDP43 aggregate continues to aggregate over time, it begins to precipitate out of solution. Photos of the samples at times 0, 300, 500, and 1000 minutes are included to show eGFP-TDP43 aggregate falling out of solution.

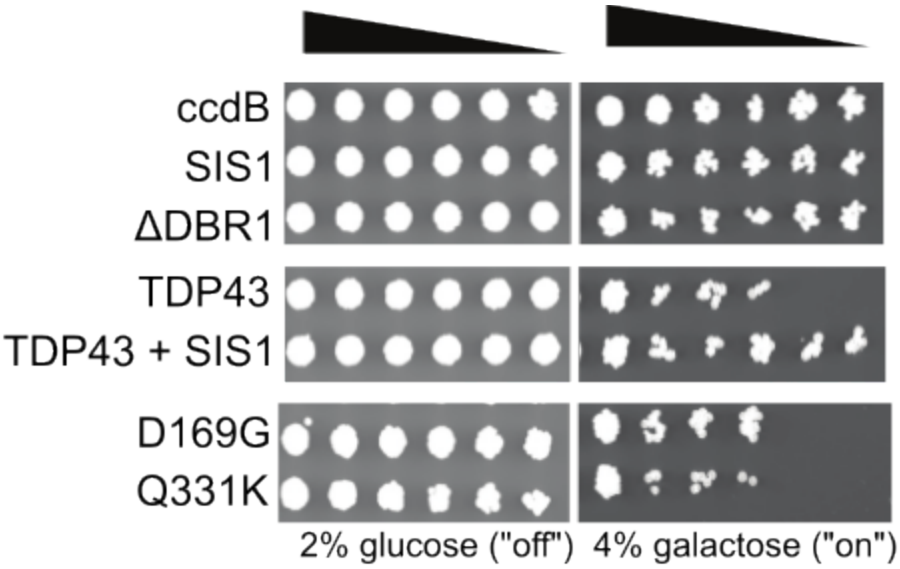

Supplementary Figure 3. Spotting assay demonstrates the recovery of growth in the cytotoxic TDP43-DsRED expressing yeasts by the over expression of SIS1, and the deletion of DBR1.

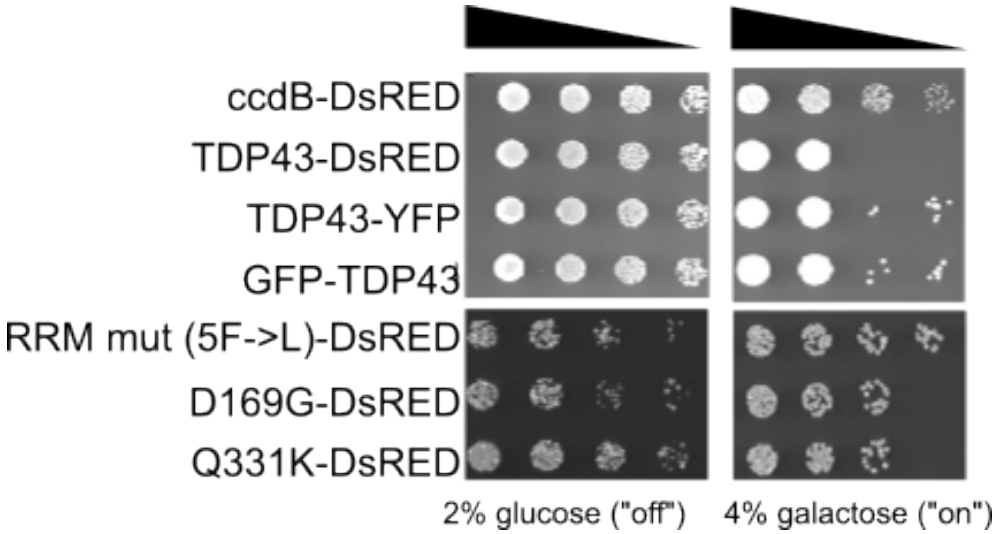

Supplemental Figure 4. The fluorescent protein fused to TDP43 can be on the N- or C-terminal end, and more than one type of fluorescent protein can be used and still retain a cytotoxic phenotype in yeast.

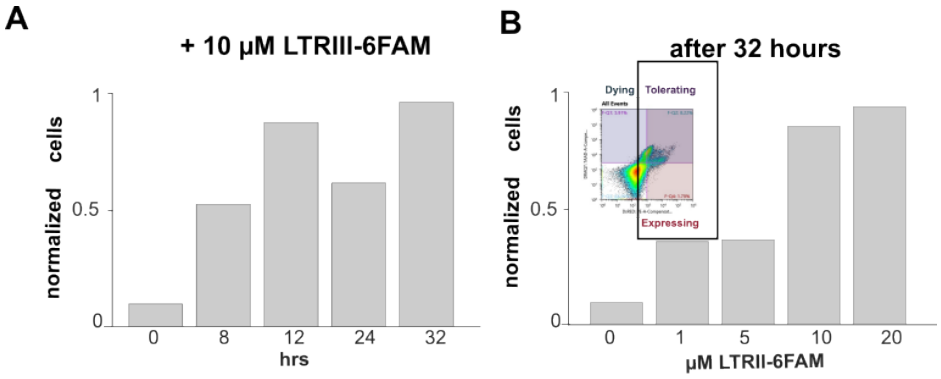

Supplemental Figure 5. **A replicate of Figure 1 D, E.** A. A time course of the normalized % cells tolerating and expressing TDP43-DsRED per 100,000 yeast cells based on DsRED and DRAQ7 intensity. B. A dosage curve of the normalized % cells tolerating and expressing TDP43-DsRED per 100,000 yeast cells based on DsRED and DRAQ7 intensity.

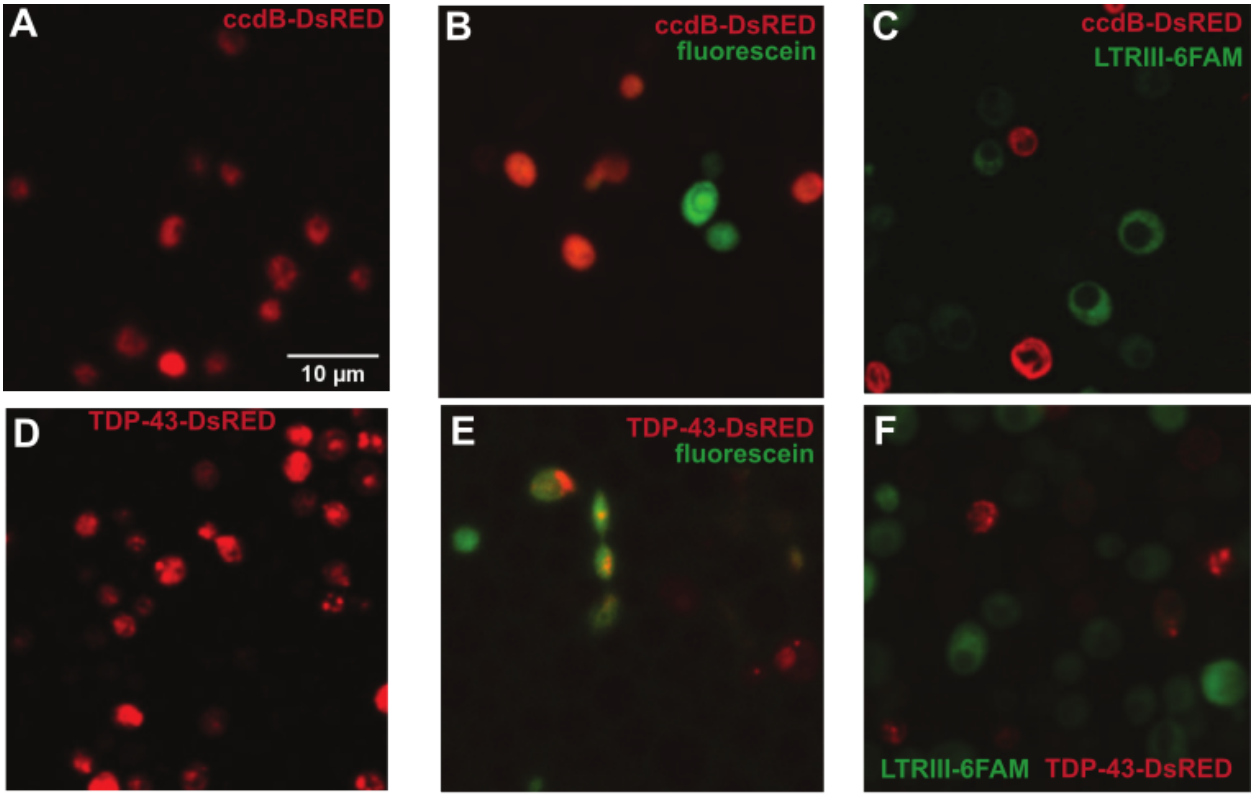

Supplementary Figure 3. G-quadruplexes and fluorescein (green) enter the yeast cytoplasm when added to the yeast media. A. ccdB-DsRED expressing yeast, with no added rG4s or fluorophore dyes confocal microscopy. B. ccdB-DsRED yeast with 10 µM fluorescein. c. ccdB-DsRED yeast with 10 µM LTRIII-6FAM. D. TDP43-DsRED expressing yeast, with no added rG4s or fluorophore dyes confocal microscopy. E. TDP43-DsRED yeast with 10 µM fluorescein. F. TDP43-DsRED yeast with 10 µM LTRIII-6FAM.

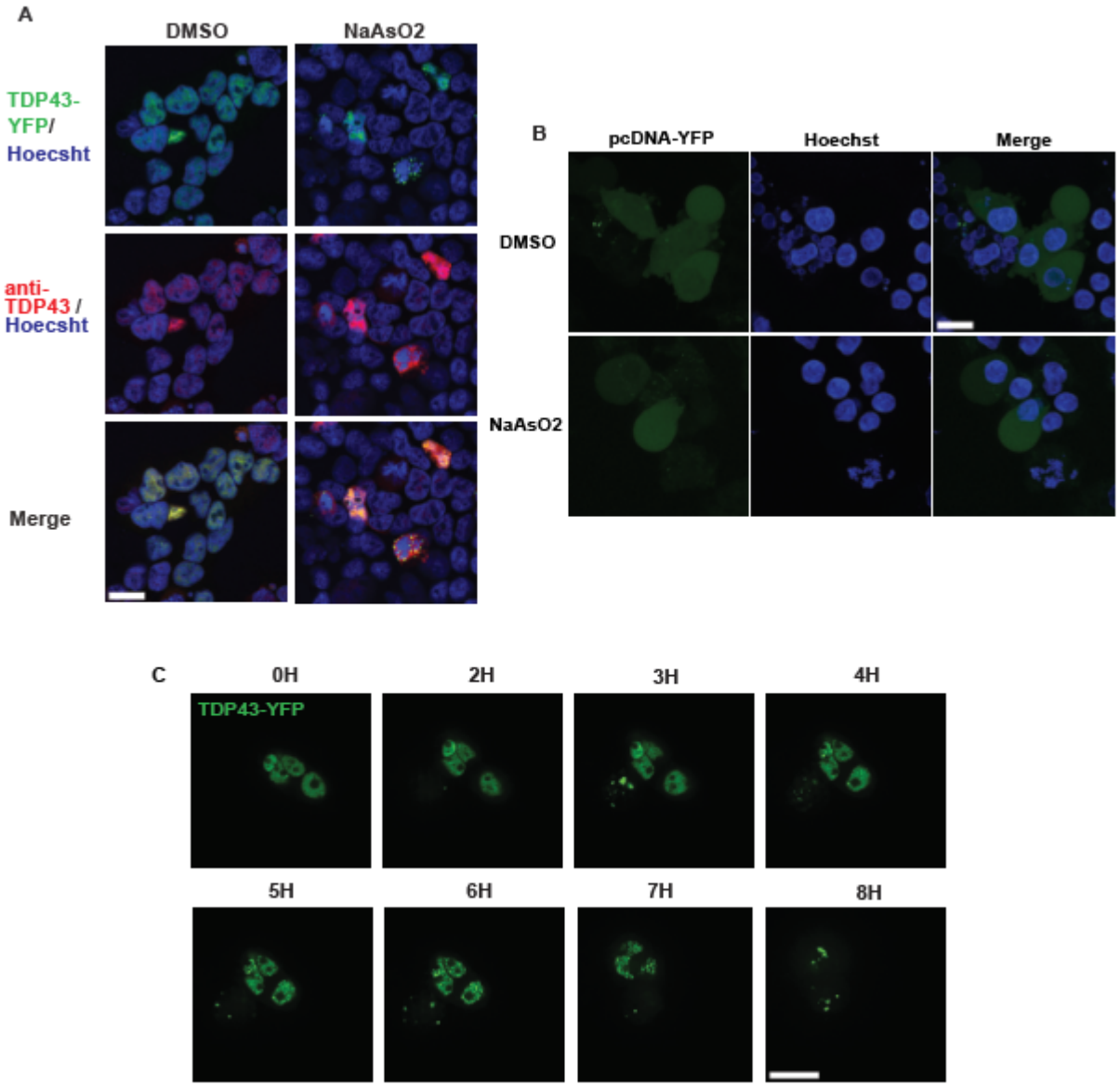

Supplementary Figure 7. Oxidative stress induction in over-expressed, stable TDP43 in HEK293T293T cells. A. Immunostaining shows colocalization of stable overexpressing HEK293T-TDP43-YFP (green) and anti-TDP43 Alexa-fluor 647 (red), Hoechst nuclear label (blue), 40x, scale bar = 20 µm. B. Empty vector pcDNA-YFP transfected into HEK293T cells and addition of $NaAsO_2$ showed no aggregation of off target fluorescence. C. Dose-dependent live confocal imaging was taken over 8 h. When treated with 50 µM $NaAsO_2$, nuclear and cytoplasmic TDP43 inclusions are observed in the HEK293T-TDP43-YFP model within 4 h. $NaAsO_2$ concentration was dropped to 15 µM to prolong disease-like aggregation state.

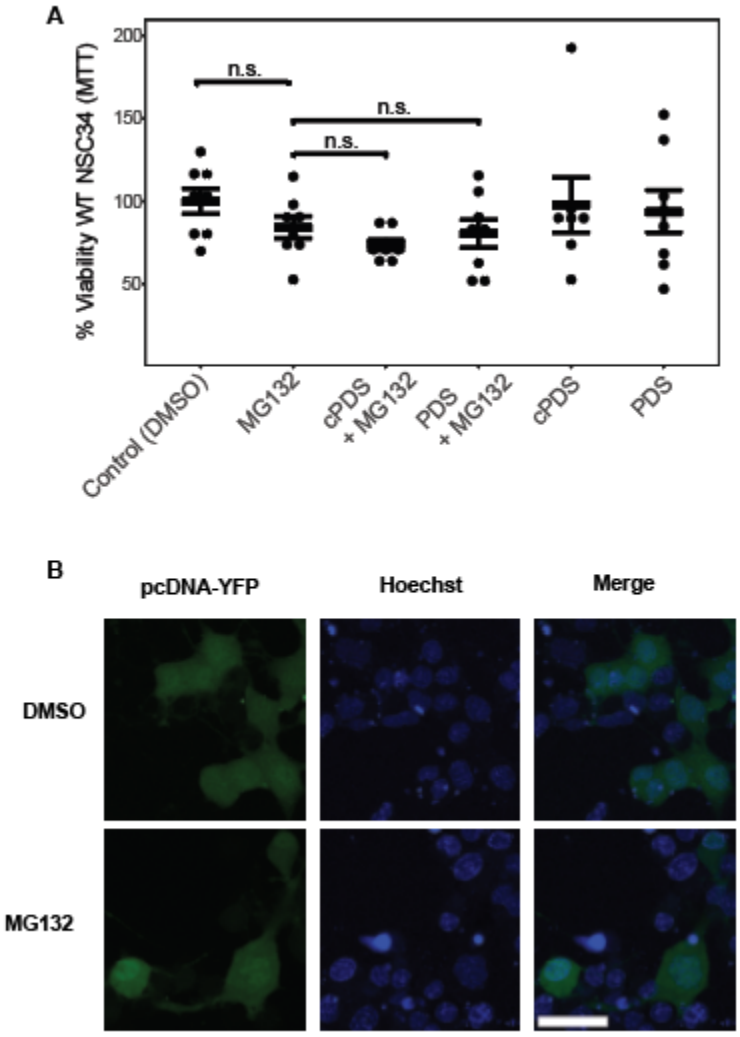

Supplemental Figure 8. WT NSC34 and transfected pcDNA -YFP show insignificant cell death or aggregation under proteasomal stress. A. WT NSC34 MTT in the presence of G4 binders PDS and cPDS and MG132, n = 6. B. Overexpression of empty vector pcDNA -YFP in NSC34 cells unremarkable after addition of proteasome inhibitor, scale bar = 40 µm.